Ligand & Band Gap Engineering: Tailoring the Protocol Synthesis for Achieving High-Quality $CsPbI_3$ Quantum Dots.

Ehsan Hassanabadi,[1,2] Masoud Latifi,[2] Andrés. F. Gualdrón-Reyes,[1] Sofia Masi,[1] Seog Joon Yoon,[1,3] Macarena Poyatos,[1] Beatriz Julian-Lopez,[1] and Iván Mora-Seró[1,*]

[1] Institute of Advanced Materials (INAM), University Jaume I, Avenida de Vicent Sos Baynat, s/n, 12071 Castellón de la Plana, Castellón, Spain.

[2] Textile Engineering Department, Textile Excellence & Research Centers, Amirkabir University of Technology, Hafez Ave., Tehran 1591634311, Iran.

[3] Department of Chemistry, College of Natural Science, Yeungnam University, 280 Daehak-Ro, Gyeongsan, Gyeongbuk 38541, Republic of Korea

*Corresponding author: sero@uji.es

Abstract

Hot-injection has become the most extended method used for the synthesis of perovskite quantum dots (QDs) with an enormous interest for the application in optoelectronic devices. However, there are some aspects of the chemistry involved in this synthesis that have not been completely investigated. In this work, we synthesized ultra-high stable $CsPbI_3$ QDs for more than 15 months by controlling two main parameters: synthesis temperature and the concentration of capping ligands. By increasing the capping ligand concentration during the QDs synthesis, we were able to grow $CsPbI_3$ in a broad range of temperatures, improving the photophysical properties of QDs when the synthesis temperature raises up. We reached the maximum photoluminescence quantum yield (PLQY) of 93 % for a synthesis conducted at 185 ºC, establishing an efficient surface passivation to decrease the density of non-radiative recombination sites. Under this optimized synthesis conditions, deep red LEDs with External Quantum Efficiency (EQE) higher than 6% are achieved. This performance is higher than the reported $CsPbI_3$ QDs-LEDs containing standard capping agents, without additional elements or farther element exchange. We show that it is possible to produce stable $CsPbI_3$ QDs with high PLQY and red emission beyond the requirement for red color from the Rec. 2020 standards.

1. Introduction

Halide perovskite colloidal quantum dots (QDs), with tunable band gap under quantum confinement regime, are considered very promising materials for the next generation of a broad range of optoelectronic devices, such as high-quality displays,[1] lasers,[2-4] light-emitting diodes,[5] photodetectors,[6] solar cells.[7-10] This interest is based on their high photoluminescence quantum yield (PLQY), bandgap tunability in the entire visible region, and narrow emission line widths.[11-16] Among the different halide perovskite QD materials, $CsPbI_3$ black phase is the inorganic Pb halide perovskite with the lowest bandgap, ~1.80 eV (~1.73 eV in bulk), favorable for both solar cells[8] and light emitting diodes (LEDs).[17, 18] A record in the external quantum efficiency (EQE) of 21% is achieved for red LEDs based on mixed-anions $CsPbBr_{3-x}I_x$,[19] highlighting the potentiality of these materials. However, it is still a challenge to obtain deep red $CsPbI_3$ LEDs, efficient and stable.[20] The main problem is the phase stability of $CsPbI_3$ black phase, that in bulk crystals transforms quickly into non-perovskite yellow δ-phase, presenting a wider band gap to be inactive under photoexcitation.[10] These features reduce the PLQY of perovskite. Nevertheless, the stability of the $CsPbI_3$ perovskite is significantly increased when this material is synthesized as nanoparticles due to the contribution of the surface energy.[10]

However, $CsPbI_3$ exhibits a blueshift in the band gap compared with the bulk counterpart due to quantum confinement limits partially its application for the deep red emission or as light harvester in perovskite QD solar cells.[10] Quantum confinement can be reduced by increasing the QDs size for approaching to the bulk band gap, without declining the red pure color, raising up the synthesis temperature.[10] Nonetheless, the formation of bigger $CsPbI_3$ QDs is restricted by some synthetic conditions. Recent reports have highlighted the difficulty of synthesizing $CsPbI_3$ QDs at temperatures higher than 180-185 °C, because the lead halide precursor is not well solubilized.[10, 21] In the case of $CsPbBr_3$ QDs, the precipitation temperature is extended to higher values by increasing the concentration of OA and OLA in the reaction mixture.[21] The synthesis of bigger QDs with narrower band gap and lower full width at half maximum (FWHM) has been achieved, but with a reduced PLQY and stability.[10, 22] In order to overcome these issues, several methods have been mainly considered: i) incorporation of bromide anions to prepare $CsPbBr_{3-x}I_x$ mixed halide perovskites;[23] ii) metal doping with Ag^+,[24] Bi^{3+},[25] Cd^{2+},[26] Mn^{2+},[27, 28] Sn^{2+},[26] Sr^{2+},[29, 30] or Zn^{2+},[26] iii) purification of the $CsPbI_3$ black phase QDs by using polar solvents such as methyl acetate (MeOAc) or ethyl acetate (EtOAc),[10, 31] and (iv) postsynthetic treatments by using water or ZnI_2-hexane solutions.[32, 33] These methods can improve different properties as size dispersion, material stability, PLQY and/or the LED performance. Interestingly, the repair of the defective QDs surface provided by the fourth strategy is critical for boosting mainly PLQY, making that the QDs posttreatment is well established to enhance the quality of the final product. Unfortunately, the enhancement of the QDs properties has, in some cases, the collateral cost of the blue-shift of the band gap, which remains a big deal. An optimized synthesis

of $CsPbI_3$ QDs, with suitable optical, structural, and electronic properties, is envisioned as the current synthesis lead to low performances in LEDs. For instance, the use of standard $CsPbI_3$ black phase QDs as active layer in the standard LEDs architecture (ITO/PEDOT/p-TPD/perovskite/TPBI/LiF/Al) has provided an external quantum efficiency (EQE) around 2.3-2.5%.[30, 34] This performance is lower than those of the LEDs based on mixed halide (I/Br) perovskite or doped perovskite, or compared with more complex architectures.[19, 29, 35] Hence, it has been difficult the preparation of long-term stable deep red $CsPbI_3$ with high PLQY, narrow FWHM and good electrical properties at the same time. By understanding the chemistry behind the QDs synthesis, these fascinating features could be unlocked and prepare high-quality materials. However, a chemical limitation of perovskite QDs stems from their high surface-to-volume ratio, and in turn from the large number of atoms or ions on the surface that are not coordinated.[36] These surface defects act as traps for photogenerated excitons, which causes non-radiative recombination and quenches the photophysical features.[22, 36] In this sense, surface passivation of QDs is a key point to minimize the non-radiative recombination. Accordingly, it is expected that the PLQY, the stability of the nanocrystals and performance of fabricated devices could be improved, with an enhanced passivation.[30, 37]

Herein, we systematically study the impact of the synthesis temperature and capping ligand concentration on the band gap, size distributions, PLQY, PL FWHM, and stability of $CsPbI_3$ black phase (hereafter called only $CsPbI_3$) QDs, synthesized by hot-injection method, and integrated as active layer in LEDs. We demonstrate that oleylammonium oleate (OLM), produced from the combination between oleic acid (OA) and oleylamine (OLA) ligands, is the determinant species to stabilize the lead precursors during synthesis[38] and promote the surface passivation of QDs. By raising up the OA and OLA concentration into the mixture reaction, we achieved the successful QDs synthesis at higher temperatures and efficient passivation of surface defects for higher performance. With these considerations, we produced $CsPbI_3$ QDs with deep red emission, high PLQY, narrow PL FWHM and ultra-high stability for more than 15 months. In this line, the photophysical properties of our QDs are competitive with previous reports of high-quality $CsPbI_3$ QDs.[13, 30, 32-34] We also observed improved red-emissive LEDs performances, with an EQE = 6% with a similar turn-on voltage compared to state-of-the-art devices in the same conditions.[30] Moreover, the chromaticity indexes from our devices were beyond the red color required for Rec. 2020 standards.[39] These findings offer a new insight about how the key synthesis parameters affecting the chemistry occurring into the QDs formation, can be properly controlled.

2. Results and discussion

In the standard hot-injection synthesis of $CsPbI_3$ QDs, in addition to the perovskite precursors, OA and OLA are added for the stabilization of the colloidal QDs.[40] Consequently, the injection of a higher OA/OLA

content allowed us to synthesize QDs at higher synthesis temperatures than conventional synthetic protocol, in order to obtain QDs with improved photophysical properties. With the purpose to understand how the temperature affects the synthesis of $CsPbI_3$ QDs, first of all, the reaction between OA and OLA was studied at different temperatures. Samples of OA, OLA and a mixture of them (1:1 molar ratio), were heated at 120 ºC under vacuum and nitrogen (mimicking the QDs synthesis conditions), and heated at the desire temperature (between 120 – 200 ºC). Then, the samples were cooled down to ambient temperature and analyzed by ^{1}H NMR (Nuclear Magnetic Resonance) spectroscopy. We excluded the use of 1-ODE due to this reagent is a non-coordinating solvent and do not take part in the reaction, but generates extra peaks in NMR analysis. Figure 1a shows the comparison between the ^{1}H NMR spectra of OA, OLA and the OA/OLA mixture prepared at ambient temperature. The resonance due to the proton from the carboxylic acid group of OA appears at chemical shift (δ) of 12.04 ppm, while the resonance due to the protons of amine group of OLA appears at δ = 1.01 ppm (denoted with *). When the reagents are mixed together, the signal corresponding to the proton of the carboxylic group disappears and the signal at δ = 1.01 ppm shifts to 8.6 ppm (denoted with *'), due to the protonation of the amine group ($-NH_2$) in favor of the ammonium one ($-NH_3^+$). The resonances of the methylene groups also shift, compared to the spectra of the starting materials, due to a different chemical environment. These results corroborate the generation of a new species, namely oleylammonium oleate (OLM), even at room temperature, formed by the protonation of OLA.[21, 41] Then, by heating the OA/OLA mixture at 80 °C and 120 °C and then cooling down to room temperature, it is clear that the triplets corresponding to the α-CH_2 resonances next to the carbonyl (2'), ammonium (19') functionalities of OLM remain unchanged and there is a negligible shift of the signal from the NH_3^+ group (Figure 1b). This fact is an evidence that the reaction, under these conditions, fully transforms the initial OA and OLA into OLM.

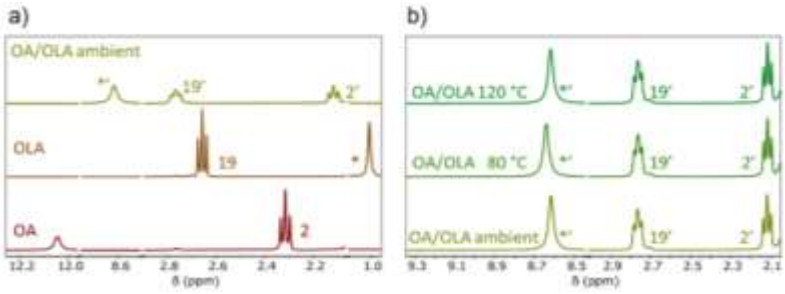

Figure 1. (a) ^{1}H NMR spectra ($CDCl_3$, 400 MHz, 25 °C) of OA and OLA capping ligands and their mixture to follow the formation of OLM at room temperature. (b) Comparison of the ^{1}H NMR spectra ($CDCl_3$, 400 MHz, 25 °C) of the mixture at ambient temperature, 80 and 120 °C. Asterisks added into the figures 1b and 1c denote the proton associated to amine group from OLA (*), and ammonium functionality from OLM (*').

By increasing the temperature of the OA/OLA mixture from 120 °C to 190 °C, collecting their corresponding ^{1}H NMR spectra (Figure 2a), the intensity of the triplets belonging to the α-CH_2 resonances next to the ammonium and to the carbonyl functionalities of OLM (19' and 2', respectively), either decrease or change shape, from triplet to multiplet, and concomitantly a new multiplet centered at δ 3.20 ppm appears. Moreover, the appearance of a new peak at δ 7.1 ppm is associated to the formation of an amide as the product of the condensation reaction (denoted as *''). [21, 42]This result is in good agreement with the decrease of the signal associated to ammonium group at 8.6 ppm (Figure 2b). In order to confirm the formation of the amide, we intentionally synthesized N-oleyl-oleamide (NOA) by mixing OA and OLA at 190 °C [38] under vacuum overnight and characterized by ^{1}H and ^{13}C NMR the final product (Figure S1a). The spectra of the synthesized product perfectly match with of the mixture of reagents at 190 ºC, thus confirming the presence of NOA. This by-product has been reported to appear at 160 °C during the synthesis of $CsPbX_3$ (X = Cl, Br, I).[43] Moreover, in comparison with the individual liquid capping ligands (OLA and OA), the aspect of the mixture changes from a viscous liquid to a white solid, passing from a mixture of liquid and solid state (Figure S1b). OLM is more viscous than OA and OLA at room temperature.

The amide compound, which has the melting point of around 50 ºC, emerges as white solids when it is mixed with OLM at room temperature. The white solid was not observed neither during the synthesis nor in the NMR tube due to the presence of octadecene and $CDCl_3$, respectively, both able to dissolve the amide. All these findings are not in line with the previous mechanisms proposed, for which the progressive increase of the temperature induces the protonation of oleate by oleylammonium at temperatures as high as 100 °C (Figure 2c (i)).[21, 41] This discrepancy could be due to the preparation of the NMR samples. If traces of water remain during the NMR sample preparation, the amide by-product could be dissociated, affording the reagents (Figure 2c (i)) and leading to different species in the mixture reaction. By conducting the synthesis at high temperatures under inert atmosphere, the condensation product NOA is formed (Figure 2c (ii)), as we estimated also by an NMR quantitative analysis, see Table 1. By integrating the corresponding NMR peaks (Figure S2a-f) and considering the concentration (or volume) of OA and OLA added during the QDs preparation, we quantitatively calculated that the concentration of OLM and NOA. It is observed that the concentration of the former decreases while that of the later increases with the temperature, see Table 1 and Table S1.

Table 1. NMR quantitative analysis of the evolution of different amounts of OA and OLA (1:1 molar ratio), OLM and NOA products at different temperatures. OA and OLA are initially fully transformed into OLM, see Figure 2c (i), and finally part of OLM is transformed into NOA, see Figure 2c (ii).

Temperature (° C)	Initial number of moles of OLM (= OA or OLA) (mmol)	Number of moles of OLM after transformation (mmol)	Number of moles of NOA after transformation (mmol)	Conversion of OLM to NOA (%)
170	4.6	3.4	1.2	26
180	9.1	4.0	5.1	56
185	12.2	4.5	7.7	63
190	12.2	4	8.2	67

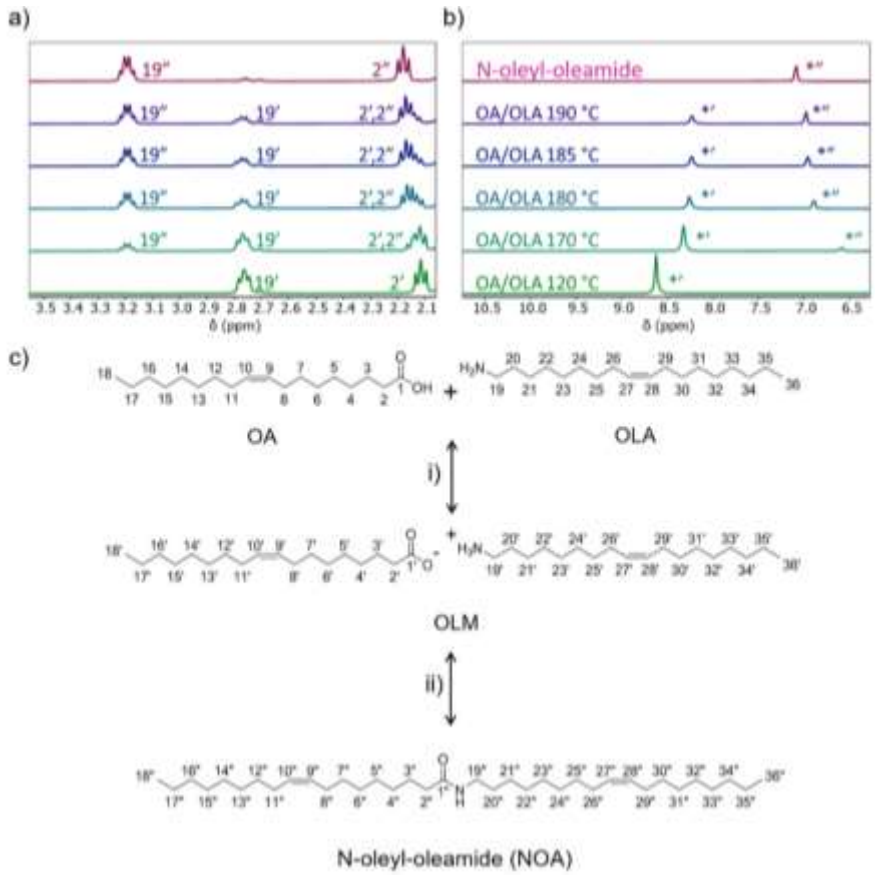

Figure 2. ^{1}H NMR spectra of the OA/OLA 1:1 molar ratio mixtures ($CDCl_3$, 400 MHz, 25 °C) at different temperatures, showing the formation of N-oleyl-oleamide from the OLM at (a) low and (b) high chemical shift. (c) Schematic representation of the reaction between oleic acid and oleylamine to produce (i) OLM oleate and (ii) N-oleyl-oleamide (NOA). Asterisks added into Figure 2b indicate the proton associated to amide group from NOA (*'').

To stabilize the lead halide precursor during the QDs synthesis, we took into account the NMR results. We modified the synthetic protocol by increasing both the concentration of OA and OLA[21, 44-46] as the reaction temperature increases.[10, 47] Four temperatures (170, 180, 185, and 190 °C) were used for the $CsPbI_3$

QDs synthesis, by varying the concentrations of OA and OLA, always in a 1:1 molar ratio, see Table 1.[40] In all the cases, $CsPbI_3$ QDs were successfully prepared, including the synthesis at higher temperatures, see Figure S3. In order to avoid the problems observed in the QDs synthesis at temperatures higher than 180-185 °C, where precursor is not well solubilized and precipitated,[10, 21] it is needed to increase the concentration of OA and OLA in order to increase the amount of OLM, see Table 1. The spontaneous organization of the long aliphatic chain of the OLM coordinating the lead iodide precursor, can react with the Cs-oleate and form the $CsPbI_3$ QDs. Consequently, the presence of OLM into the mixture reaction is essential to promote the stabilization of $CsPbI_3$ QD. If the concentration of OLM is not increased (via the increase of OA and OLA precursors, see Figure 2c (i)), when the synthesis temperature is enhanced, the final amount of available OLM decreases with temperature due to the fact that higher synthesis temperatures accelerate the transformation of OLM to produce NOA through the condensation reaction (formation of amide bound), see Figure 2c (ii). The lead iodide precursor was dissolved in the OLM, which resulted in a complex of PbI_2 coordinated by the oleylammonium iodide and Pb-oleate, as authenticated by the transparent lemon color of the solution. When the amount of OLM is not high enough to produce this coordination, an orange-reddish precipitate is obtained due to the PbI_2 precipitation. This fact was commonly observed when the QDs synthesis was attempted at T>180ºC, with no further increase of the standard OA and OLA concentration. The increase in OA and OLA concentration needs to consider the partial loss of OLM transformed into NOA. This loss increases as the temperature rises, see the percentage of OLM conversion into NOA in Table 1. Consequently, we increased the OA/OLA concentration between 20-60 % in comparison with the conventional hot-injection method, in order to allow the synthesis at higher temperatures that indeed modified the properties of the QDs, as we discuss below.

Moreover, OLM does not only play a key role in the QDs synthesis, but also in their passivation and consequently, in the final QDs properties.[36, 48, 49] Thus, at higher temperatures, more amount of OA and OLA is needed to ensure that enough OLM is available to first fully stabilize the PbI_2 allowing the QDs synthesis and later passivate the QD surface. Therefore, it is expected that a higher amount of OLM favors the QDs surface passivation with important implication in the QD properties and also in the long-term stability, as non-passivated surface I^- vacancies are the main responsible for the self-degradation of QDs.[50]

Figures 3a-d show the TEM images of synthesized $CsPbI_3$ QDs obtained with the conditions reported in Table 1. In all the cases, nanocrystals with nanocube shape are obtained. The rise of the synthesis temperature increases the average nanoparticle size between 9.1 nm and 13.2 nm, but decreases the QDs size distribution, see Table 2 and Figure S4. Thus, all the synthesized QDs exhibit quantum confinement regime (QCR) effects as the Bohr diameter for $CsPbI_3$ is around 13 nm.[40] After hot-injection of Cs^+ species to PbI_2 precursor, a broad population of small and big QDs are formed, which depends on the concentration of dissolved Cs^+, Pb^{2+} and I^- species into the reaction medium. Koolyk et al,[51] reported a size standard

distribution of $CsPbI_3$ QDs between 2.9-3.4 nm for a QDs sizes between 7.5-10.5 nm, by increasing the reaction time from 4 to 20 s (before quenching). In the same line, Zhao et al,[52] reported a size distribution in $CsPbI_3$ QDs between 1.7-2.2 nm for QDs sizes between 13.9-15.3 nm. In our case, the reaction time is limited to 5 s, obtaining a lower size distribution between 1.23-1.65 nm for QDs size between 9.1-13.2 nm (Table 2). We deduced that the increase of the synthesis temperature instead of the reaction time can mediate a fast consume of above species supporting the growth of small QDs to reach the size of larger ones, which present a slower particle growth rate.[51] In our case, this phenomenon can favors that the QDs population is in the same size range, narrowing the particle size distribution.[21, 51] Moreover, the increase of the temperature produces an increase of the NOA formation that could increase the viscosity, decreasing the diffusion of the reactants. Thus, the proven progressive increase in NOA formation with the temperature, see Table 1, could produce a higher limitation of the reaction by diffusion, which is proved to be one of the requirements of narrowing the particle size distribution.[53, 54]

Table 2. Summary of the different structural and optical parameters of the $CsPbI_3$ QDs analyzed in this work. Size dispersion is calculated considering the standard deviation respect the QD size.

Synthesis temperature (°C)	Size of QD (nm)	Size Standard distribution (nm)	Size Dispersion (%)	PL peak (nm)	PL FWHM (nm) (meV)	Initial PLQY (%)	Reduction of PLQY after 15 months (%)
170	9.14	1.65	18.05	677	44.6 (121)	87	21
180	10.60	1.84	17.36	681	42.4 (113)	91	16
185	12.84	1.67	13.01	685	37.6 (100)	93	7
190	13.16	1.23	9.34	687	36.0 (94.8)	92	8

Furthermore, XRD profiles of the $CsPbI_3$ QDs were also acquired, exhibiting two main diffraction peaks at Bragg angles around 14.2° and 28.7°, see Figure 3f. These signals are associated to the (100) and (200) planes from the perovskite lattice, respectively, which are characteristic signals of the cubic phase (ICSD 540752).[55, 56] This crystalline phase has been reported to be preferential when the $CsPbI_3$ QDs synthesis is conducted at temperatures between 170-190 °C,[16, 40] and it is retained under room conditions due to the high surface energy generated in the confined QDs.[10, 57] According to these results, we deduced that the increase of capping ligand concentration in the conventional hot-injection method, see Table 1, is essential for the stabilization of $CsPbI_3$ QDs at higher reaction temperatures, with bigger and more homogeneous particle size, presenting in all the cases, a nanocube shape and a crystalline cubic phase.

In an attempt to synthesize QDs at 200 ºC, we kept increasing the amount of OA and OLA added to the mixture reaction similar as we carried out for the previous syntheses. Unfortunately, the PbI_2 precipitation was observed, avoiding the QDs preparation. At this stage, we deduced that higher transformation of OLM to NOA conducted at this temperature showed a stronger influence on the QDs synthesis than the increase of capping ligands content, blocking the QDs growth. Under this observation, it is clear that the QDs synthesis at higher temperatures ≥ 200 ºC demands extra modifications to our synthetic route, where the increase of capping ligands ratio is not enough to mediate the stabilization of the lead precursor (see below).

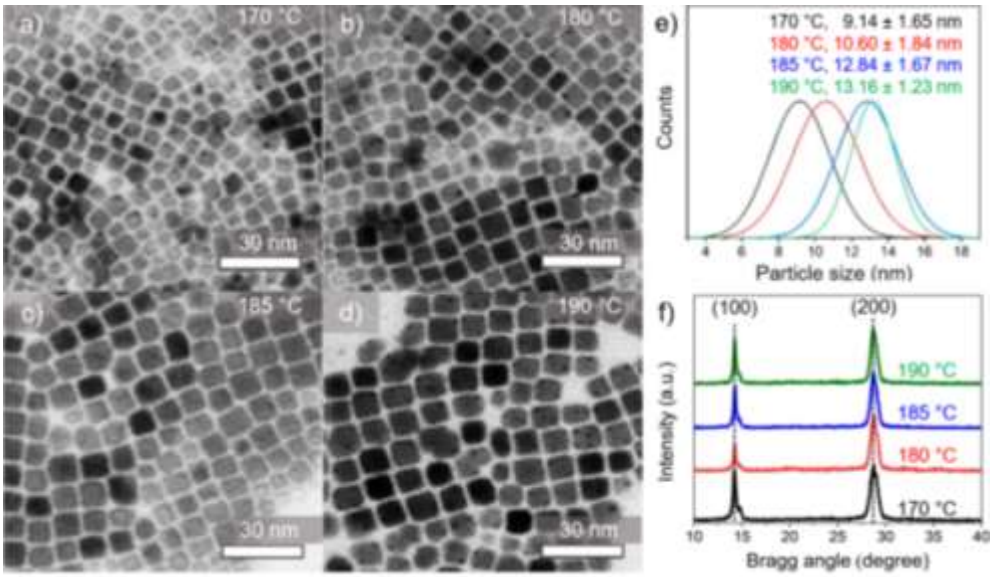

Figure 3. (a-d) TEM images, (e) particle size distributions obtained from TEM and (f) XRD patterns of the $CsPbI_3$ QDs solutions obtained at diverse synthesis temperatures: 170, 180, 185 and 190°C.

Given that the $CsPbI_3$ QDs size was directly influenced by the synthesis temperature, it was also expected that this parameter impact also on the optical features of these materials. The PL peak positions of the $CsPbI_3$ QDs prepared at different temperatures are depicted in Figure 4a. As the synthesis temperature increases, the emission peak positions were red-shifted. This trend indicates the narrowing of the bandgap, E_g, due to a relaxation of the QCR as the size of QDs increases. Moreover, the bigger the $CsPbI_3$ QDs, the narrower the full width half maximum (FWHM) of the corresponding PL peaks (Figure 4b), obtaining values as low as 36 nm (94.8 meV) for QDs grown at 190ºC, see Table S2. This value is lower than the conventional FWHM reported for red-emitting $CsPbI_3$ QDs (around 40 nm),[16, 58] and similar to the FWHM of near unity PLQY $CsPbI_3$ QDs synthesized by adding organic precursors (for instance, trioctylphosphine or 2,2′-iminodibenzoic acid) in accordance with a perovskite stabilization.[13, 34] This comparison infers that by a simple modification in the hot-injection method protocol without using extra chemical stabilizers, we

were able to enhance the quality of the materials. The reduction of the FWHM is in good agreement with the reduction of the QDs size dispersion, from the average size and the corresponding size standard distribution obtained by TEM images, see Table 2, Figure 3e and S4. This fact clearly demonstrates that whether the population of QDs is more prone to be in the same particle size range by increasing the synthesis temperature as we discussed above, a high density of QDs with smaller band gap (reduced QCR) will emit at same wavelength. Thus, a lower size dispersion narrows the PL FWHM, improving the color purity of $CsPbI_3$ QDs when synthesis temperature increases.

The PLQY of the $CsPbI_3$ QDs is also influenced by the synthesis parameters, see Figure 4c. By conducting the QDs synthesis at temperatures between 170-185 °C, we evidenced an increase of the PLQY to achieve a maximum value around 93 %. A small decrease of PLQY to 92 % is observed for the QDs grown at 190 ºC. After 6 months to store the QDs solutions under air atmosphere, we estimated their corresponding time-resolved PL measurements, which exhibit longer decays as synthesis temperature increases, see Figure S5. PL decay measurements were conducted after this period of time with the purpose to correlate the improved photophysical properties as PLQY of QDs with their long-term stability. The average lifetimes, τ_{avg}, estimated from the PL decays allows the calculation of the corresponding radiative and non-radiative recombination decay rate constants, K_r and K_{nr}, see Table S2 and Figure 4d. The trend observed in the PLQY, see Figure 4c, of the as-prepared QDs synthesized at different temperatures is in excellent agreement with the inverse of the K_{nr}/K_r ratio, see Figure 4e. Note that all the QDs exhibit similar K_r, but K_{nr} decreases with the synthesis temperature as temperature moves from 170 to 185 ºC, reporting a minimum at the last temperature and then a slight increase when temperature rises to 190 ºC. Consequently, the shape of K_{nr}/K_r ratio, and therefore of the PLQY, is influenced by the change of the non-radiative decay rate. As the temperature increases from 170 to 185 ºC, the non-radiative recombination channels are reduced, increasing slightly when the temperature varies from 185 ºC to 190 ºC. We attribute the reduction of the non-radiative recombination channels with the different QDs synthesis conditions to a different effective passivation of the QD surface by OLM, as we discuss below.

For carrying out the QDs synthesis at temperatures ≥ 200 ºC, it was necessary to introduce an extra modification to our synthetic route. Instead of stabilizing PbI_2 at 120 °C, we conducted the stabilization of lead precursor at desire temperature just before the Cs-oleate injection. Under this condition, we minimized the time needed to induce the conversion of OLM to NOA into the mixture reaction. Thus, we were able to synthesize QDs at 210 and 230 ºC, with PLQY and FWHM ~ 90 % and 32 nm, respectively. Even though these photophysical properties show near values to the suitable condition one (185 ºC), this procedure requires further optimization. However, we proved once again with this finding that the synthesis and stabilization of $CsPbI_3$ QDs can be guaranteed by ensuring the presence of enough content of OLM. In the

same line, we concluded that OLM mediates the passivation of defects on QDs surface.[49] Note that, in the different synthesis conditions, we modified the QDs size and consequently the surface that needs to be passivated, see Table S1, and the amount of available OLM for the surface passivation, see Table 1. With these two parameters it is possible to calculate the available OLM per surface unit, see in Table S1, as the OLM/surface ratio. This ratio follows the same trend than the PLQY, pointing to an increase of OLM passivating agent as the origin of the PLQY enhancement. It is clear that the reduction of surface defects by ligand passivation is a key point to improve the photophysical features of QDs, similar to the surface treatment performed by postsynthetic protocols.[32, 33] In the same line, very recently, Hao et al.[9] have also reported the most recent performance record for QDs solar cells, 16.6%, using perovskite QDs synthesized with an excess of OA.

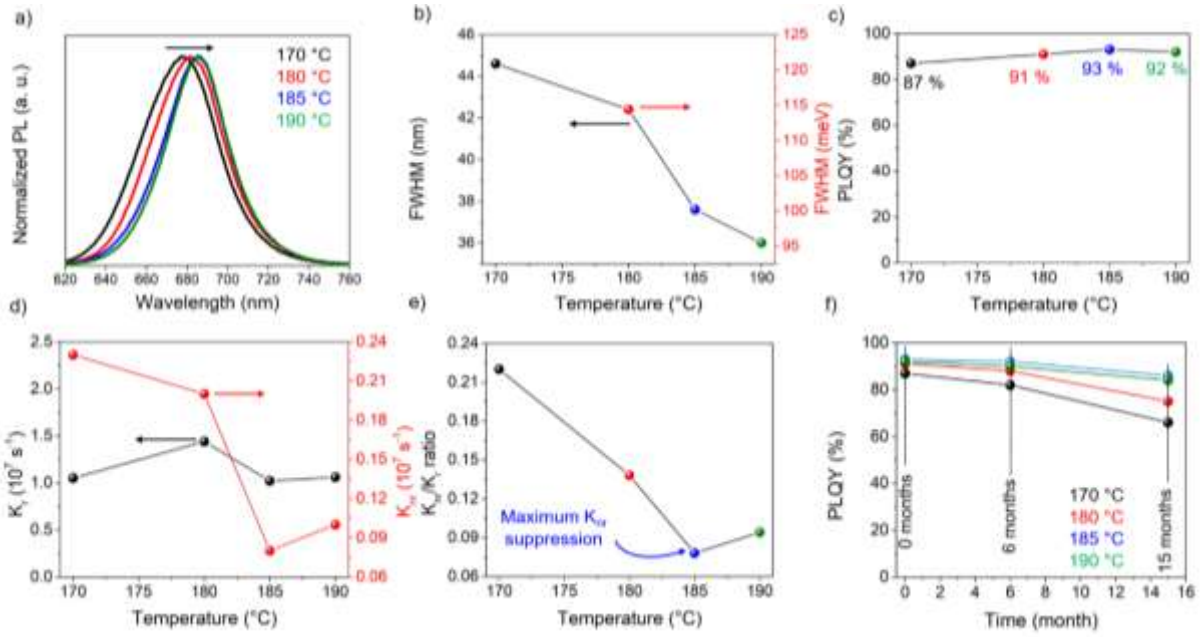

Figure 4. (a) Normalized photoluminescence spectra, (b) Full width at half-maximum (FWHM), (c) absolute photoluminescence quantum yield (PLQY) of as prepared QDs solutions. (d) Radiative (K_r) and non-radiative recombination (K_{nr}) decay constants, and their corresponding (e) K_{nr}/Kr ratio for QDs solutions after 6 months of storage. (f) PLQY stability for 15 months for $CsPbI_3$ QDs synthesized at different synthesis temperatures.

Beyond the positive effect of the improved QD passivation on the PLQY, this passivation also has a remarkable effect in the long-term stability of $CsPbI_3$ QDs. We tracked the PLQY of perovskite QDs, stored under air atmosphere into fridge, after 6 and 15 months, see Figure 4f. In these periods of time, the PLQY just decreased 3 and 7 % of the original value for QDs presenting the highest PLQY, the ones synthesized at 185 ºC. This behavior is in good agreement with the K_{nr}/K_r ratio established in Figure 4e, where the

maximum suppression of non-radiative recombination channels was reached. In addition, the reduction of the initial PLQY after 15 months is inversely proportional to the initial PLQY, see Table 2 and Table S3. This stability is well above the current stability of commercially available $CsPbI_3$ and $CsPbBr_3$, which normally present an expiring date of 3 months. Hence, we conclude that the proper passivation of surface defects provided by OLM enhances both PLQY and the stability of QDs in a long-term.

The improvement of the photophysical properties of $CsPbI_3$ QDs by using our synthetic route allowed us to explore these materials as light emitters for the fabrication of LEDs. Considering the high PLQY as the main feature of the synthesized QDs, a high performance in LED can be favored.[59, 60] Devices were prepared using the likely most extended perovskite LED architecture, ITO/PEDOT:PSS/poly-TPD/$CsPbI_3$/TPBi/LiF/Al see Figure 5a-b,[61] that ensures a proper electron and hole injection into the perovskite QD active layer.[62] We have fabricated LEDs just varying the active layer, by using $CsPbI_3$ QDs synthesized at different temperatures. In order to ensure the dependence of the LED performance on the photophysical properties of QDs, avoiding the influence of external factors from the device preparation (QDs concentration, thickness of active, electron and hole transporter layers, etc.), we fabricated multiple LED devices by using the same and different batches of each kind of QDs solutions for device optimization. As it is shown in Figure 5c, we observe that the maximum EQE obtained for the LEDs QDs presents exactly the same behavior that the K_{nr}/K_r recombination rate ratio by varying the synthesis temperature, Figure 4e. In this context, we achieved the highest EQE performance with the QDs synthesized at 185 ºC, due to the reduction of the non-radiative recombination sites into QDs. All the devices present a roll-off effect in the current above 100 $mA \cdot cm^{-2}$ as it is commonly observed in perovskite LEDs.[63] The luminance (L) was also dependent of the synthesis conditions (Figure 5d). LEDs presenting the lowest turn-on voltage (V_{ON}), 4.8 V, were prepared with QDs synthesized at 185 °C.

Considering the previously reported record performance for non-modified $CsPbI_3$ QDs that presents performance values of 2.25-2.5% EQE, L of 400 Cdm^{-2} and as V_{ON} 4.5-6 V,[30, 34] our devices present similar values of the LED parameters. However, after contact optimization reported in the supporting information, a champion $CsPbI_3$-LED device showing a maximum EQE and L values around 6.02 % and 587 $Cd \cdot m^{-2}$, was obtained, see Figure 5e and 5f respectively. The maximum current from the champion device was 1381 $mA \cdot cm^{-2}$, Figure 5f, producing a red light, see inset of Figure 5g, with a turn-on voltage of 4.8 V. This optimized device showed better performance than previous reports, as for example Sr^{2+}-modified $CsPbI_3$ QDs LEDs (EQE = 5.92 %, V_{ON} = 9.2 V),[30] KBr-passivated $CsPbBr_{3-x}I_x$ QDs LEDs (EQE = 3.55 %, V_{ON} = 4.6),[64] and relatively close to the performance of highly flexible $CsPbI_3$ QDs LEDs (EQE = 8.2 %, V_{ON} = 2 V).[65] Furthermore, the $CsPbI_3$ LEDs fabricated in this study corresponds to a deep red color that have the CIE chromaticity coordinates (x,y), beyond the red emission coordinates according with the Rec. 2020

standards for red color (0.708, 0.292), [39] see Figure 5g,h and Table S4. Hence, we widely demonstrate that the maximum reduction of non-radiative recombination channels into QDs reached by controlling the synthesis temperature and capping ligand concentration opens the door to the improvement of the optoelectronic properties of perovskites to be competitive in the fabrication of highly-performance LEDs with purer color.

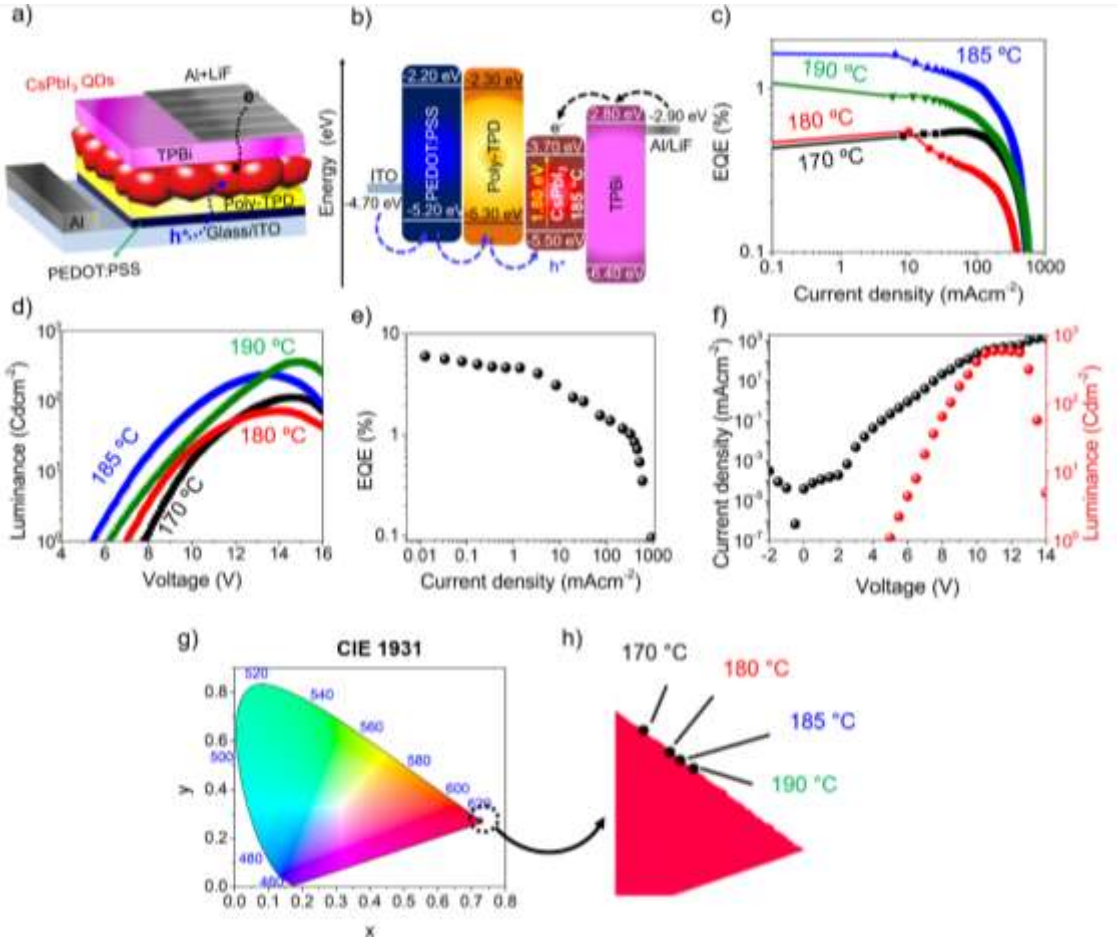

Figure 5. (a) Schematic diagram and (b) relative energy band positions of a $CsPbI_3$-LED configuration. Performance characterization of devices: (c) EQE, and (d) luminance of $CsPbI_3$-LED fabricated from different perovskite quantum dots by varying the synthesis temperature. (e) Maximum EQE (f) current/luminance for the champion $CsPbI_3$-LED device using quantum dots synthesized at 185 °C. Inset of Figure 5f shows the photograph of the $CsPbI_3$-LED device under operation. (g, h) CIE Chromaticity at different temperatures.

3. Conclusions

By increasing the ligand concentration in the conventional protocol for hot-injection method, we unlocked the synthesis of $CsPbI_3$ QDs with enhanced photophysical properties: higher PLQY, narrower PL FWHM, deep red color (narrower bandgap) and enhanced long term stability. We elucidated that OA and OLA are fully transformed into OLM during the synthesis, being this species the key factor for enabling the synthesis at higher temperatures and performing an efficient passivation of QD surfaces. $CsPbI_3$ synthesized with a higher amount of OLM per unit surface area of QDs present higher PLQY and longer QD stability. Enhanced OLM passivation induces a decrease of the non-radiative recombination channels, prolonging the highest material stability for at least 15 months, evidencing only a decrease in the PLQY around 7 % after this period for QDs synthesized at 185 ºC. By understanding the chemistry behind the QDs synthesis, we applied these materials into LEDs fabrication, reaching an EQE around 6 % and a chromaticity index beyond the Rec. 2020 standards for deep red. The performance of the fabricated LEDs is higher than the previous reported ones with the same standard architectures, containing standard capping agents, without additional elements or farther element exchange. Hence, we demonstrate that our synthetic protocol can provide high-quality and ultra-stable $CsPbI_3$ QDs that can be effectively employed in highly efficient optoelectronic devices.

ASSOCIATED CONTENT

Supporting Information. Experimental setup, ^{1}H-NMR and ^{13}C-NMR spectra of OA/OLA mixtures heated at different temperatures; histograms, photoimages, PL decay and tables of the corresponding band gap, FWHM, lifetime, and PLQY stability of the $CsPbI_3$ QDs synthesized at diverse synthesis temperatures.

AUTHOR INFORMATION

ORCID

Andres F. Gualdrón-Reyes: 0000-0002-0208-9235

Sofia Masi: 0000-0002-7373-1627

Seog Joon Yoon: 0000-0002-8921-9062

Macarena Poyatos: 0000-0003-2000-5231

Beatriz Julian-Lopez: 0000-0003-1019-776X

Iván Mora-Seró: 0000-0003-2508-0994

Author contribution

E.H. and I. M.-S. conceived the project. E.H. and S.M. optimized the LEDs. E.H. synthesized QDs with the collaboration of B.J.-L. E.H. and A.F.G.R characterized the QDs optical properties and the devices. S. M. and M. P contributed to the NMR characterization. M.L. and S.J.Y. assisted in the work analysis. E.H., A. F. G. R., S. M. and I. M.-S. wrote the manuscript. All the authors contributed to the discussions.

Corresponding Author

*Address correspondence to this author: sero@uji.es, Twitter: @IvanMoraSero,

DECLARATION OF INTERESTS

The authors declare no competing interests

ACKNOWLEDGMENT

This work was supported by European Research Council (ERC) via Consolidator Grant (724424–No-LIMIT), EU (FEDER) under project TEC2017-85912-C2-2, and Generalitat Valenciana via Prometeo Grant Q-Devices (Prometeo/2018/098). We acknowledge the SCSIE from the University of Valencia for providing TEM facilities.

References:

1. Q. Zhou, Z. Bai, W.-g. Lu, Y. Wang, B. Zou and H. Zhong, *Advanced Materials*, 2016, **28**, 9163-9168.
2. Y. Xu, Q. Chen, C. Zhang, R. Wang, H. Wu, X. Zhang, G. Xing, W. W. Yu, X. Wang, Y. Zhang and M. Xiao, *Journal of the American Chemical Society*, 2016, **138**, 3761-3768.
3. H. Zhu, Y. Fu, F. Meng, X. Wu, Z. Gong, Q. Ding, M. V. Gustafsson, M. T. Trinh, S. Jin and X. Y. Zhu, *Nature Materials*, 2015, **14**, 636-642.
4. J. Navarro-Arenas, I. Suárez, V. S. Chirvony, A. F. Gualdrón-Reyes, I. Mora-Seró and J. Martínez-Pastor, *The Journal of Physical Chemistry Letters*, 2019, **10**, 6389-6398.
5. Z.-K. Tan, R. S. Moghaddam, M. L. Lai, P. Docampo, R. Higler, F. Deschler, M. Price, A. Sadhanala, L. M. Pazos, D. Credgington, F. Hanusch, T. Bein, H. J. Snaith and R. H. Friend, *Nature Nanotechnology*, 2014, **9**, 687-692.
6. L. Dou, Y. Yang, J. You, Z. Hong, W.-H. Chang, G. Li and Y. Yang, *Nature Communications*, 2014, **5**.

7. Z. Zolfaghari, E. Hassanabadi, D. Pitarch-Tena, S. J. Yoon, Z. Shariatinia, J. van de Lagemaat, J. M. Luther and I. Mora-Seró, *ACS Energy Letters*, 2018, **4**, 251-258.
8. F. Li, S. Zhou, J. Yuan, C. Qin, Y. Yang, J. Shi, X. Ling, Y. Li and W. Ma, *ACS Energy Letters*, 2019, DOI: 10.1021/acsenergylett.9b01920, 2571-2578.
9. M. Hao, Y. Bai, S. Zeiske, L. Ren, J. Liu, Y. Yuan, N. Zarrabi, N. Cheng, M. Ghasemi, P. Chen, M. Lyu, D. He, J.-H. Yun, Y. Du, Y. Wang, S. Ding, A. Armin, P. Meredith, G. Liu, H.-M. Cheng and L. Wang, *Nature Energy*, 2020, **5**, 79-88.
10. A. Swarnkar, A. R. Marshall, E. M. Sanehira, B. D. Chernomordik, D. T. Moore, J. A. Christians, T. Chakrabarti and J. M. Luther, *Science*, 2016, **354**, 92-95.
11. G. Xing, N. Mathews, S. S. Lim, N. Yantara, X. Liu, D. Sabba, M. Grätzel, S. Mhaisalkar and T. C. Sum, *Nature Materials*, 2014, **13**, 476-480.
12. Y. Fu, H. Zhu, C. C. Stoumpos, Q. Ding, J. Wang, M. G. Kanatzidis, X. Zhu and S. Jin, *ACS Nano*, 2016, **10**, 7963-7972.
13. F. Liu, Y. Zhang, C. Ding, S. Kobayashi, T. Izuishi, N. Nakazawa, T. Toyoda, T. Ohta, S. Hayase, T. Minemoto, K. Yoshino, S. Dai and Q. Shen, *ACS Nano*, 2017, **11**, 10373-10383.
14. D. Shi, V. Adinolfi, R. Comin, M. Yuan, E. Alarousu, A. Buin, Y. Chen, S. Hoogland, A. Rothenberger, K. Katsiev, Y. Losovyj, X. Zhang, P. A. Dowben, O. F. Mohammed, E. H. Sargent and O. M. Bakr, *Science*, 2015, **347**, 519-522.
15. H. Diab, G. Trippé-Allard, F. Lédée, K. Jemli, C. Vilar, G. Bouchez, V. L. R. Jacques, A. Tejeda, J. Even, J.-S. Lauret, E. Deleporte and D. Garrot, *The Journal of Physical Chemistry Letters*, 2016, **7**, 5093-5100.
16. G. Nedelcu, L. Protesescu, S. Yakunin, M. I. Bodnarchuk, M. J. Grotevent and M. V. Kovalenko, *Nano Letters*, 2015, **15**, 5635-5640.
17. Q. V. Le, J. B. Kim, S. Y. Kim, B. Lee and D. R. Lee, *The Journal of Physical Chemistry Letters*, 2017, **8**, 4140-4147.
18. J. Gan, J. He, R. L. Z. Hoye, A. Mavlonov, F. Raziq, J. L. MacManus-Driscoll, X. Wu, S. Li, X. Zu, Y. Zhan, X. Zhang and L. Qiao, *ACS Energy Letters*, 2019, **4**, 1308-1320.
19. T. Chiba, Y. Hayashi, H. Ebe, K. Hoshi, J. Sato, S. Sato, Y.-J. Pu, S. Ohisa and J. Kido, *Nature Photonics*, 2018, **12**, 681-687.
20. N. Pradhan, *The Journal of Physical Chemistry Letters*, 2019, **10**, 5847-5855.
21. G. Almeida, L. Goldoni, Q. Akkerman, Z. Dang, A. H. Khan, S. Marras, I. Moreels and L. Manna, *ACS Nano*, 2018, **12**, 1704-1711.
22. S. B. Naghadeh, B. Luo, Y.-C. Pu, Z. Schwartz, W. R. Hollingsworth, S. A. Lindley, A. S. Brewer, A. L. Ayzner and J. Z. Zhang, *The Journal of Physical Chemistry C*, 2019, **123**, 4610-4619.
23. R. J. Sutton, G. E. Eperon, L. Miranda, E. S. Parrott, B. A. Kamino, J. B. Patel, M. T. Hörantner, M. B. Johnston, A. A. Haghighirad, D. T. Moore and H. J. Snaith, *Advanced Energy Materials*, 2016, **6**, 1502458.
24. M. Lu, X. Zhang, X. Bai, H. Wu, X. Shen, Y. Zhang, W. Zhang, W. Zheng, H. Song, W. W. Yu and A. L. Rogach, *ACS Energy Letters*, 2018, **3**, 1571-1577.
25. P. K. Nayak, M. Sendner, B. Wenger, Z. Wang, K. Sharma, A. J. Ramadan, R. Lovrinčić, A. Pucci, P. K. Madhu and H. J. Snaith, *Journal of the American Chemical Society*, 2018, **140**, 574-577.
26. W. van der Stam, J. J. Geuchies, T. Altantzis, K. H. W. van den Bos, J. D. Meeldijk, S. Van Aert, S. Bals, D. Vanmaekelbergh and C. de Mello Donega, *Journal of the American Chemical Society*, 2017, **139**, 4087-4097.
27. W. Liu, Q. Lin, H. Li, K. Wu, I. Robel, J. M. Pietryga and V. I. Klimov, *Journal of the American Chemical Society*, 2016, **138**, 14954-14961.
28. J. Zhu, X. Yang, Y. Zhu, Y. Wang, J. Cai, J. Shen, L. Sun and C. Li, *The Journal of Physical Chemistry Letters*, 2017, **8**, 4167-4171.
29. M. Lu, X. Zhang, Y. Zhang, J. Guo, X. Shen, W. W. Yu and A. L. Rogach, *Advanced Materials*, 2018, **30**, 1804691.

30. J.-S. Yao, J. Ge, K.-H. Wang, G. Zhang, B.-S. Zhu, C. Chen, Q. Zhang, Y. Luo, S.-H. Yu and H.-B. Yao, *Journal of the American Chemical Society*, 2019, **141**, 2069-2079.
31. E. M. Sanehira, A. R. Marshall, J. A. Christians, S. P. Harvey, P. N. Ciesielski, L. M. Wheeler, P. Schulz, L. Y. Lin, M. C. Beard and J. M. Luther, *Science Advances*, 2017, **3**, eaao4204.
32. Y. Liu, F. Li, Q. Liu and Z. Xia, *Chemistry of Materials*, 2018, **30**, 6922-6929.
33. F. Li, Y. Liu, H. Wang, Q. Zhan, Q. Liu and Z. Xia, *Chemistry of Materials*, 2018, **30**, 8546-8554.
34. J. Pan, Y. Shang, J. Yin, M. De Bastiani, W. Peng, I. Dursun, L. Sinatra, A. M. El-Zohry, M. N. Hedhili, A.-H. Emwas, O. F. Mohammed, Z. Ning and O. M. Bakr, *Journal of the American Chemical Society*, 2017, **140**, 562-565.
35. S. Yuan, Z.-K. Wang, M.-P. Zhuo, Q.-S. Tian, Y. Jin and L.-S. Liao, *ACS Nano*, 2018, **12**, 9541-9548.
36. Y. Chen, S. R. Smock, A. H. Flintgruber, F. A. Perras, R. L. Brutchey and A. J. Rossini, *Journal of the American Chemical Society*, 2020, DOI: 10.1021/jacs.9b13396.
37. X. Shen, Y. Zhang, S. V. Kershaw, T. Li, C. Wang, X. Zhang, W. Wang, D. Li, Y. Wang, M. Lu, L. Zhang, C. Sun, D. Zhao, G. Qin, X. Bai, W. W. Yu and A. L. Rogach, *Nano Letters*, 2019, **19**, 1552-1559.
38. V. K. Ravi, P. K. Santra, N. Joshi, J. Chugh, S. K. Singh, H. Rensmo, P. Ghosh and A. Nag, *The Journal of Physical Chemistry Letters*, 2017, **8**, 4988-4994.
39. R. Zhu, Z. Luo, H. Chen, Y. Dong and S.-T. Wu, *Optics Express*, 2015, **23**, 23680.
40. L. Protesescu, S. Yakunin, M. I. Bodnarchuk, F. Krieg, R. Caputo, C. H. Hendon, R. X. Yang, A. Walsh and M. V. Kovalenko, *Nano Letters*, 2015, **15**, 3692-3696.
41. H. Huang, J. Raith, S. V. Kershaw, S. Kalytchuk, O. Tomanec, L. Jing, A. S. Susha, R. Zboril and A. L. Rogach, *Nature Communications*, 2017, **8**.
42. C. Cara, A. Musinu, V. Mameli, A. Ardu, D. Niznansky, J. Bursik, M. A. Scorciapino, G. Manzo and C. Cannas, *Crystal Growth & Design*, 2015, **15**, 2364-2372.
43. R. Grisorio, M. E. Di Clemente, E. Fanizza, I. Allegretta, D. Altamura, M. Striccoli, R. Terzano, C. Giannini, M. Irimia-Vladu and G. P. Suranna, *Nanoscale*, 2019, **11**, 986-999.
44. Z. Liu, Y. Bekenstein, X. Ye, S. C. Nguyen, J. Swabeck, D. Zhang, S.-T. Lee, P. Yang, W. Ma and A. P. Alivisatos, *Journal of the American Chemical Society*, 2017, **139**, 5309-5312.
45. A. Pan, B. He, X. Fan, Z. Liu, J. J. Urban, A. P. Alivisatos, L. He and Y. Liu, *ACS Nano*, 2016, **10**, 7943-7954.
46. J. De Roo, M. Ibáñez, P. Geiregat, G. Nedelcu, W. Walravens, J. Maes, J. C. Martins, I. Van Driessche, M. V. Kovalenko and Z. Hens, *ACS Nano*, 2016, **10**, 2071-2081.
47. A. Dutta, S. K. Dutta, S. Das Adhikari and N. Pradhan, *Angewandte Chemie International Edition*, 2018, **57**, 9083-9087.
48. R. Grisorio, E. Fanizza, I. Allegretta, D. Altamura, M. Striccoli, R. Terzano, C. Giannini, V. Vergaro, G. Ciccarella, N. Margiotta and G. P. Suranna, *Nanoscale*, 2020, **12**, 623-637.
49. M. I. Bodnarchuk, S. C. Boehme, S. ten Brinck, C. Bernasconi, Y. Shynkarenko, F. Krieg, R. Widmer, B. Aeschlimann, D. Günther, M. V. Kovalenko and I. Infante, *ACS Energy Letters*, 2018, **4**, 63-74.
50. A. F. Gualdrón-Reyes, J. Rodríguez-Pereira, E. Amado-González, J. Rueda-P, R. Ospina, S. Masi, S. J. Yoon, J. Tirado, F. Jaramillo, S. Agouram, V. Muñoz-Sanjosé, S. Giménez and I. Mora-Seró, *ACS Applied Materials & Interfaces*, 2019, **12**, 914-924.
51. M. Koolyk, D. Amgar, S. Aharon and L. Etgar, *Nanoscale*, 2016, **8**, 6403-6409.
52. Q. Zhao, A. Hazarika, L. T. Schelhas, J. Liu, E. A. Gaulding, G. Li, M. Zhang, M. F. Toney, P. C. Sercel and J. M. Luther, *ACS Energy Letters*, 2020, **5**, 238-247.
53. L. Cademartiri, J. Bertolotti, R. Sapienza, D. S. Wiersma, G. von Freymann and G. A. Ozin, *The Journal of Physical Chemistry B*, 2006, **110**, 671-673.
54. D. V. Talapin, A. L. Rogach, M. Haase and H. Weller, *The Journal of Physical Chemistry B*, 2001, **105**, 12278-12285.

55. M. Chen, Y. Zou, L. Wu, Q. Pan, D. Yang, H. Hu, Y. Tan, Q. Zhong, Y. Xu, H. Liu, B. Sun and Q. Zhang, *Advanced Functional Materials*, 2017, **27**, 1701121.
56. G. E. Eperon, G. M. Paternò, R. J. Sutton, A. Zampetti, A. A. Haghighirad, F. Cacialli and H. J. Snaith, *Journal of Materials Chemistry A*, 2015, **3**, 19688-19695.
57. Q. Zhao, A. Hazarika, L. T. Schelhas, J. Liu, E. A. Gaulding, G. Li, M. Zhang, M. F. Toney, P. C. Sercel and J. M. Luther, *ACS Energy Letters*, 2019, **5**, 238-247.
58. L. Protesescu, S. Yakunin, S. Kumar, J. Bär, F. Bertolotti, N. Masciocchi, A. Guagliardi, M. Grotevent, I. Shorubalko, M. I. Bodnarchuk, C.-J. Shih and M. V. Kovalenko, *ACS Nano*, 2017, **11**, 3119-3134.
59. H. Wang, X. Zhang, Q. Wu, F. Cao, D. Yang, Y. Shang, Z. Ning, W. Zhang, W. Zheng, Y. Yan, S. V. Kershaw, L. Zhang, A. L. Rogach and X. Yang, *Nature Communications*, 2019, **10**.
60. Y. Liu, T. Wu, Y. Liu, T. Song and B. Sun, *APL Materials*, 2019, **7**, 021102.
61. C. Zou, C.-Y. Huang, E. M. Sanehira, J. M. Luther and L. Y. Lin, *Nanotechnology*, 2017, **28**, 455201.
62. F. Krieg, S. T. Ochsenbein, S. Yakunin, S. ten Brinck, P. Aellen, A. Süess, B. Clerc, D. Guggisberg, O. Nazarenko, Y. Shynkarenko, S. Kumar, C.-J. Shih, I. Infante and M. V. Kovalenko, *ACS Energy Letters*, 2018, **3**, 641-646.
63. X. Dai, Z. Zhang, Y. Jin, Y. Niu, H. Cao, X. Liang, L. Chen, J. Wang and X. Peng, *Nature*, 2014, **515**, 96-99.
64. J.-N. Yang, Y. Song, J.-S. Yao, K.-H. Wang, J.-J. Wang, B.-S. Zhu, M.-M. Yao, S. U. Rahman, Y.-F. Lan, F.-J. Fan and H.-B. Yao, *Journal of the American Chemical Society*, 2020, **142**, 2956-2967.
65. M. Lu, H. Wu, X. Zhang, H. Wang, Y. Hu, V. L. Colvin, Y. Zhang and W. W. Yu, *ChemNanoMat*, 2018, **5**, 313-317.

TOC Figure